



HAL
open science

Assessing and optimizing the performance of infrasound networks to monitor volcanic eruptions

Dorianne Tailpied, Alexis Le Pichon, Emanuele Marchetti, Jelle Assink, Sylvie Vergniolle

► **To cite this version:**

Dorianne Tailpied, Alexis Le Pichon, Emanuele Marchetti, Jelle Assink, Sylvie Vergniolle. Assessing and optimizing the performance of infrasound networks to monitor volcanic eruptions. *Geophysical Journal International*, 2016, 208 (1), pp.437-448. 10.1093/gji/ggw400 . cea-02107725

HAL Id: cea-02107725

<https://cea.hal.science/cea-02107725>

Submitted on 23 Apr 2019

HAL is a multi-disciplinary open access archive for the deposit and dissemination of scientific research documents, whether they are published or not. The documents may come from teaching and research institutions in France or abroad, or from public or private research centers.

L'archive ouverte pluridisciplinaire **HAL**, est destinée au dépôt et à la diffusion de documents scientifiques de niveau recherche, publiés ou non, émanant des établissements d'enseignement et de recherche français ou étrangers, des laboratoires publics ou privés.

Assessing and optimizing the performance of infrasound networks to monitor volcanic eruptions

Dorianne Tailpied,¹ Alexis Le Pichon,¹ Emanuele Marchetti,² Jelle Assink³
and Sylvie Vergniolle⁴

¹CEA, DAM, DIF, F-91297 Arpajon, France. E-mail: tailpied.dorianne@gmail.com

²Dipartimento di Scienze della Terra (UNIFI), Università di Firenze, I-50121 Florence, Italy

³Royal Netherlands Meteorological Institute (KNMI), P.O. Box 201, NL-3730 AE, De Bilt, The Netherlands

⁴Institut de Physique du Globe de Paris, IPGP, CNRS, Université Paris 7, F-75005 Paris, France

Accepted 2016 October 19. Received 2016 October 14; in original form 2016 February 24

SUMMARY

We propose a numerical modeling technique based on a frequency-dependent attenuation relation to assess, quantify and optimize the performance of any arbitrary infrasound network to monitor explosive sources such as volcanic eruptions. Simulations are further enhanced by including realistic sources and propagation effects. We apply our approach to both hemispheres by considering the Euro-Mediterranean and the Eastern Australian regions. In these regions, we use quasi-permanent infrasound signals from Mt. Etna recorded in Tunisia and from Mt. Yasur recorded in New Caledonia. These well-instrumented volcanoes offer a unique opportunity to validate our attenuation model. In particular, accurate comparisons between near- and far-field recordings demonstrate the potential of the proposed methodology to remotely monitor volcanoes. A good agreement is found between modeled and observed results, especially when incorporating representative 10 m s^{-1} wind perturbations in the atmospheric specifications according to previous campaign measurements. To optimize the network layout in order to ensure the best monitoring of the volcanoes, we proceed through a grid search to find optimum locations of an additional array. We show that adding one array at an appropriate location in both regions under study could significantly improve detections half of the year. The application of the proposed methodology can provide in near real-time a realistic confidence level of volcanic eruption detections, useful to mitigate the risk of aircrafts encountering volcanic ash.

Key words: Volcano seismology; Wave propagation; Acoustic properties; Atmospheric effects (volcano); Remote sensing of volcanoes; Volcano monitoring.

INTRODUCTION

Produced by a large variety of natural and anthropogenic phenomena, infrasounds are acoustic waves below the 20 Hz threshold of human hearing (e.g. Evers & Haak 2010). These signals can propagate over large distances through the atmosphere due to low attenuation in acoustic waveguides (Sutherland & Bass 2004). Infrasound propagation can be described by multiple reflections between the different atmospheric layers. Several types of ducting are possible in the atmosphere. The first one occurs at thermospheric altitudes (i.e. higher than 100 km) due to the increase of temperature and thus of acoustic speed. Another ducting results from interactions between winds and sound speed at middle altitude (i.e. in the stratosphere). It presents strong seasonal variations caused by wind reversals, especially during the equinoxes. Some tropospheric arrivals can also be detected when wind jets within the troposphere are strong enough to overcome the sound speed decrease as a result of the adiabatic lapse

rate. However, the thermospheric waveguide is more absorptive and therefore not as relevant as tropospheric and stratospheric ducting in long-range sound propagation. Depending on the wind and temperature conditions throughout the lower and middle atmosphere, ducting can then be either reinforced or reduced (de Groot-Hedlin *et al.* 2010; Mutschlener & Whitaker 2010).

Interest in propagation studies has been revived since the Comprehensive Nuclear Test Ban Treaty (CTBT, <http://www.ctbto.org/>) has adopted infrasound as one of its verification technologies in 1996. Designed to ensure compliance with the CTBT, the International Monitoring System (IMS) intends to provide a reliable monitoring system for the detection and the location of any nuclear explosions. In this context, the IMS infrasound network was designed to detect and localize at least a one kiloton of TNT threshold with two stations (Brachet *et al.* 2010; Christie & Campus 2010). Even though not yet fully established, the IMS infrasound network has already demonstrated its capability to permanently detect and

locate a large number of anthropogenic and geophysical events (e.g. Campus & Christie 2010). In particular, as the infrasound signals are able to propagate over long distances, this technique is valuable to remotely monitor volcanoes especially in regions where ground-based and space-borne observations are sparse or not available (Dabrowa *et al.* 2011; Matoza *et al.* 2011b; Fee & Matoza 2013). For example, satellites are not able to constantly cover the atmosphere as their capability may be impaired by clouds. In this case, infrasound is a great complementary technique to cover the gaps in satellite data. In this context, it even allows to identify potential hazard for aircraft safety. As infrasound signals are associated with the ejection of material in the atmosphere and the release of conduit overpressure, they are a good indicator that a volcanic eruption has occurred. Near-field experiments have already proven that infrasound measurements can provide reliable and useful information about the source processes involved in the eruptive activity (Vergnolle & Brandeis 1994; Marchetti *et al.* 2009; Johnson & Ripepe 2011; Ripepe *et al.* 2013). At local recording distances, acoustic amplitude and power, frequency content and signal envelope are easily quantified. These parameters are then used to yield constraints on the physics of volcanic explosions such as the geometry of magmatic gas bubbles or the size of the vent. Moreover, under several assumptions on the signal radiation from the vent, these parameters could also be used to infer mass ejection velocities (Woulff & McGetchin 1976; Delle Donne & Ripepe 2012). The estimated eruption velocities serve as input for numerical models of plume rise, which is a key input in simulations of atmospheric ash dispersion (Lamb *et al.* 2015).

In order to simulate the monitoring capability of any infrasound network, it is necessary to predict the signal amplitude at any location and further assess whether the signal can be detectable above the noise level (Pilger *et al.* 2015). Simulations can further be enhanced by including source and propagation effects (e.g. source frequency, realistic atmospheric models and fine-scale atmospheric structures excluded from the current atmospheric specifications) in full-wave numerical propagation methods (Le Pichon *et al.* 2012; Hedlin & Drob 2014).

In this paper, we propose a methodology to assess at high spatiotemporal resolution (i.e. modeling the region as a $(1^\circ \times 1^\circ)$ grid, for a time period ranging from several hours to years), the detection capability of an infrasound network to monitor industrial events or geophysical surface processes such as volcanic eruptions. It allows to precisely evaluate and then optimize the performance of any infrasound network. First, we describe the modeling technique used and its implementation. The simulated detection capability of the IMS network to detect volcanic eruptions is analysed in both hemispheres through multiyear comparisons between near- and far-field recordings while incorporating realistic atmospheric uncertainties. We consider both Mt. Etna in Italy and Mt. Yasur in Vanuatu. Finally, quantitative investigations into network performance optimization are carried out in these two regions.

METHODS

Modeling technique

To model the detection capability of an arbitrary infrasound network, it is necessary to predict the signal amplitude at any required time and location, and further evaluate whether the signal can be detected at the receivers. Unlike seismic waves that propagate through the Earth where propagation conditions do not change

with time, infrasonic waves propagate through the ever-changing atmosphere. Various approaches considering empirical yield-scaling relationships derived from remote observations have been proposed (Whitaker 1995; Green & Bowers 2010). However, the conclusions of these studies may be misleading because they do not include an accurate description of the time-varying atmosphere (Fee *et al.* 2013). Infrasound can propagate over long distances without significant attenuation through atmospheric waveguides thanks to specific temperature and wind gradients. This propagation is characterized by the properties of refraction, reflection, diffraction, advection, attenuation and dispersion. Due to the generally high-frequency content of volcanic signals (>0.3 Hz) and due to atmospheric absorption at high altitudes (Bass 1995), thermospheric returns are strongly attenuated and rarely detected beyond ~ 1000 km. Under specific temperature and wind features, most of the acoustic energy can also propagate through stratospheric waveguides where refraction to the ground can be observed. Clearly captured in meteorological models, such atmospheric conditions are crucial to consider as it controls to first order where infrasound signals are expected to be detected (Evers & Haak 2010; Kulichkov *et al.* 2010; Norris *et al.* 2010; Green *et al.* 2011; Smets *et al.* 2015).

Infrasound propagation can usually be modeled by the classic acoustic ray-tracing method based on the laws of Snell-Descartes. However, several limits can be pointed out since the trajectories are purely geometric. This method becomes less precise and even inappropriate when the size of fine atmospheric structures is comparable to the acoustic wavelength (Garcés *et al.* 1998). In this context, the parabolic equation (PE) method has been used to account for diffraction and scattering due to small-scale structure in the atmosphere such as due to gravity waves that significantly affect infrasound propagation. The parabolic method is one of the most effective techniques to realistically propagate the acoustic energy over various distances in a stratified atmosphere (Lingevitch *et al.* 2002).

To quantify the infrasound network performance in high spatiotemporal resolution, a frequency-dependent attenuation relationship derived from massive range-independent PE simulations is examined (Le Pichon *et al.* 2012). It provides a basis for better understanding the role of the different factors affecting propagation predictions. Considering constant atmospheric conditions along the propagation path, at a given station M located at a distance R (km) from the source S at a reference distance of 1 km, the attenuation formula is given by:

$$A_{(M,S)} = \frac{1}{R} 10^{\frac{\alpha(f)R}{20}} + \frac{R^{\beta(f, C_{\text{eff-ratio}})}}{1 + 10^{\frac{\delta-R}{\sigma(f)}}} \quad (1)$$

where the four parameters σ , α , δ and β are calculated using a multidimensional curve-fitting approach. In the geometrical shadow zone α refers to the dissipation of the direct wave (km^{-1}), σ to the scaling distance controlling the strength of the attenuation beyond the first stratospheric bounce (km^{-1}) and δ represents the width of the shadow zone. Beyond the shadow zone, β is a dimensionless parameter that accounts for geometrical spreading and dissipation of both stratospheric and thermospheric paths. $A_{(M,S)}$ depends on both the frequency f and the effective sound speed ratio $C_{\text{eff-ratio}}$ which is defined as the ratio between the effective sound speed (maximum of sound speed plus along path wind between 30 and 60 km altitude) and the sound speed at the ground level. Beyond 200 km, the attenuation relation predicts two main scenarios: (i) upwind, when $C_{\text{eff-ratio}} < 1$, thermospheric paths dominate, (ii) downwind, when

$C_{\text{eff-ratio}} > 1$, atmospheric conditions favour long-range propagation through stratospheric waveguide.

For every 1° segment along the propagation paths, the longitudinal variations of the wind and temperature profiles are included in the simulations through $C_{\text{eff-ratio}}$ following the methodology proposed by de Groot-Hedlin and Hedlin (2014). The attenuation $A^{(i)}_{(M_i,S)}$ is computed using eq. (1) at 1° intervals along the propagation path given the local wind conditions at each step M_i . The final range-dependent attenuation is:

$$A_{(M,S)} = \prod_{i \text{ from the source } S \text{ to the station } M} \frac{A^{(i+1)}_{(M_{i+1},S)}}{A^{(i+1)}_{(M_i,S)}} \quad (2)$$

In case of constant atmospheric profiles along the propagation path, eq. (2) is equal to eq. (1). Using eqs (1) and (2), the minimum detectable source amplitude is:

$$P_{(M,S)} = \frac{N_{M(f)} \text{SNR}_M}{A_{(M,S)}(f, C_{\text{eff-ratio}})} \quad (3)$$

Eq. (3) combines the effect of the source-to-receiver distance R , the source frequency f , realistic atmospheric specifications $C_{\text{eff-ratio}}$, realistic time-varying station noise conditions $N_M(f)$ and the signal-to-noise ratio SNR_M above which signals can reliably be detected. $N_M(f)$ at the stations are derived from power spectral density noise calculation (Brown *et al.* 2014a). We also assume a SNR_M equal to 1 above which standard detection algorithms can reliably detect small-amplitude signals above the background noise (Evers & Haak 2005). For each station, M part of a given network, $P_{(M,S)}$ is calculated for a point-like source S moving around the region of interest E_S . Considering the whole network and the explored source region, the minimum detectable amplitude P is given by:

$$P = \left\{ \min_{M \in \text{Network}} \{P_{(M,S)}\} \right\}_{S \in E_S} \quad (4)$$

Setting a specific threshold, eq. (4) defines whether the source is detectable above the noise level by the network. A frequency-, site- and time-dependent noise model enables the capture of the full noise variability across the network (Brown *et al.* 2014a). The temporal and spatial variability of the atmosphere are described using the ECMWF's (European Centre for Medium-Range Weather Forecasts, part of the Integrated Forecast System cycle 38r1, <http://www.ecmwf.int/>) operational High spatial RESolution forecasts (HRES) of the winds and temperatures between 30 and 60 km. In addition, based on systematic comparisons between middle atmospheric measurements and numerical weather prediction (NWP) models, realistic wind speed uncertainties in the stratopause region (40–50 km altitude) are incorporated in the simulations. Observations in NWP models are often limited to the low atmosphere due to the lack of operational atmospheric soundings in the middle and upper atmosphere. Therefore, there is a great interest to validate atmospheric specifications using independent measurements. Under the ARISE project (Atmospheric dynamics Research InfraStructure in Europe, <http://arise-project.eu/>), measurement campaigns were conducted during 2012 and 2013 at the Haute-Provence Observatory in France (OHP, 43.93°N, 5.71°E). They aim at better describing the dynamics of the middle atmosphere. In particular, wind radiometer and Rayleigh lidar measurements allowed quantifying differences between independent collocated measurements and output of NWP models, over temporal scales ranging from days to several years (Le Pichon *et al.* 2015). It was found that the standard deviation of mean difference exceeds 5 K for the temperature (i.e. ~ 5 per cent of the sound speed), and 15–20 m s⁻¹ for the

zonal wind, between 40 and 60 km altitude. These uncertainties can even exceed 30 K for the temperature and 40 m s⁻¹ for the zonal wind in winter. These deviations can be explained by misrepresented small-scale structures in the ECMWF analyses in the range of altitude where routine observations are lacking (Kulichkov *et al.* 2010; Kulichkov & Golikova 2011; Assink *et al.* 2014a; Hedlin & Drob 2014) or either by a bias with larger scales as NWP models are designed to be a smoothed version of reality in order to sustain stability. Such uncertainties need to be considered because they have significant effect on infrasound propagation. In the following, according to these studies conducted under the ARISE project, we consider a perturbation term of 5 per cent on $C_{\text{eff-ratio}}$ (i.e. 10 m s⁻¹ on the effective sound speed).

Optimization procedure

Optimizing the layout of an arbitrary infrasound network is essential to ensure and enhance the coverage of a specific region throughout the year. Increasing the number of arrays and carefully choosing their location significantly affect the network detection capability. Considering non-linearity associated with geophysical inverse problems, the proposed optimization procedure is based on a direct grid search approach. This technique's objective is to find the optimum locations of additional arrays minimizing the detection thresholds in a specific region and period of interest.

Each position in the region is referred as a potential site for adding a new array. At a given location M , the minimum detectable source amplitude of the new network configuration is computed over the geographical area of interest. To quantify the improvement of the network detection capability, an averaged score F_M is calculated as:

$$F_M = \text{mean}_{j \in E_t} \left\{ \text{mean}_{i \in E_r} \left\{ \frac{P_{\text{ini}}(x_i, t_j)}{P_{\text{new}}(x_i, t_j)} \right\} \right\} \quad (5)$$

where P_{ini} and P_{new} are the initial and new detection thresholds, respectively, that depend both on the location x_i in the region E_r and at the time t_j in the observation period E_t . P_{ini} and P_{new} are averaged over the region and throughout the period of interest. The position M corresponding to the optimized network configuration is given by:

$$F_{\text{max}} = \max_{M \in E_r} \{F_M\} \quad (6)$$

RESULTS: VALIDATION OF THE SIMULATIONS

Repetitive identified anthropogenic or natural sources referred to as ground truth can be used as independent measures to validate network performance simulations (e.g. Green *et al.* 2010; Gibbons *et al.* 2015). Among naturally occurring infrasound phenomena, volcanic eruptions are unique and valuable repetitive sources for calibrating infrasound propagation models as they are often well instrumented in the near field and at regional distances (e.g. Matozo *et al.* 2011b; Assink *et al.* 2014a).

The interest in the ability of infrasound to remotely detect volcanic eruptions has been revived with the creation of the IMS network, which is unique in its global and homogeneous coverage. Significant advances in array designs and processing methods as well as the development of highly sensitive sensors and efficient wind-noise filtering systems now allow detection of low-amplitude volcanic signals from remote sources with an unprecedented precision (Brown *et al.* 2014b).

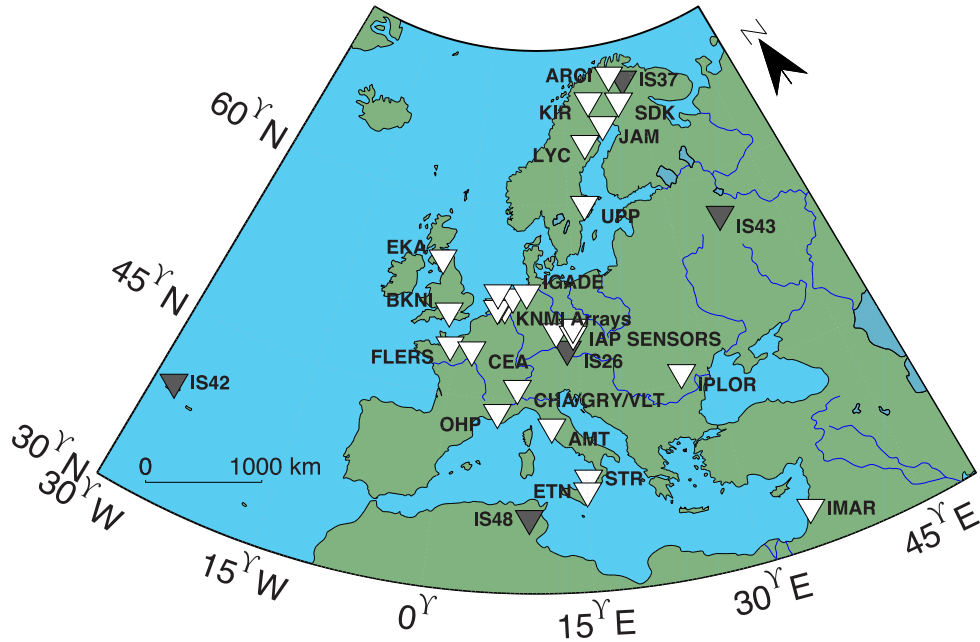


Figure 1. Geographical locations of stations used in this study. Grey and white reverse triangles indicate IMS and national arrays exploited under the ARISE project, respectively. STR and ETN stations, operated by the UNIFI in Sicily, are located less than 5 km from the volcanoes Mt. Stromboli and Mt. Etna, respectively.

Validation using repetitive volcanic infrasound from Mt. Etna, Sicily

In this part, we assess the potential of the Euro-Mediterranean region to monitor Mt. Etna volcano (37.73°N, 15.00°E; 3330 m high), by comparing near- and far-field recordings, from 2008 until 2014. Because of its regular activity, Mt. Etna represents a unique opportunity to validate the simulated detection capability of the infrasound network over the Euro-Mediterranean (Tailpied *et al.* 2013).

Observation network

In addition to the operating IMS infrasound network, other national arrays have contributed to this study within the course of the ARISE project (Fig. 1). The University of Firenze (UNIFI) actively takes part in the detection of infrasound signals in the Mediterranean region. One experimental array operated by UNIFI since 2007 September is located at the summit of Mt. Etna (ETN, 37.71°N; 15.03°E). At 5 km from the main vents, this array allows to accurately monitor its eruptions. The array processing of the ETN data consists of a delay and sum analysis-based algorithm to detect eruptions, determine the peak-to-peak pressure, and to identify the active Etna crater (Ulivieri *et al.* 2013). At long ranges, Mt. Etna is also well detected by the Tunisian IMS station (IS48, 35.80°N, 9.32°E), at about 550 km from the volcano. Processing of the IS48 data is performed using the progressive multichannel correlation (PMCC) algorithm (Cansi 1995). PMCC estimates wave front parameters (e.g. backazimuth, trace velocity and root-mean-square amplitude) of coherent plane waves for a given time window using correlation time delays between successive array element triplets. In case of major eruptions, other IMS stations can also record infrasound signals from Mt. Etna such as IS43 in Russia, at 2680 km from the volcano (Tailpied *et al.* 2013). The detection of Mt. Etna at the stations strongly depends on the prevailing wind and temperature conditions. Even if during the majority of winter months,

signals are not detected at IS48, the detection capability of Mt. Etna at station IS48 over the years is the best for monitoring purposes.

In Fig. 2(a), we present simulations of the geographical coverage of the minimum detectable source amplitude in Europe, while considering the IMS network only and completed with the experimental stations. Simulations are carried out at 1.6 Hz, which is consistent with Mt. Etna frequency, and we consider one-station coverage. The used attenuation relation (Le Pichon *et al.* 2012) allows predicting the first stratospheric shadow zone unlike other previous methods (Whitaker 1995; Green & Bowers 2010).

As expected, the network performance follows the seasonal circulation of the stratospheric zonal winds. In winter, sources located at the west of the stations will be detected with amplitudes as low as 10 Pa, while considering one-station coverage. In summer, the strong westward stratospheric currents favour signal propagation from source located at the east. According to the strength of the wind in Fig. 2 (i.e. size of the arrows), we can highlight a stronger vortex in winter (i.e. January) than in summer (i.e. July). However, while the propagation efficiency is better in winter due to stronger jets, the detection capability is better in summer. This is emphasized by the bigger areas with smaller detection thresholds during summer when compared to the winter (*cf.* Fig. 2). For example, Mt. Etna is likely to be detected by IS48 with a threshold of 10 Pa in July. In January, detection thresholds increase up to 80 Pa (Fig. 2a). When adding all the experimental arrays to the IMS network, it significantly improves the network detection capabilities during both winter and summer. Indeed, in January and July, the covered surface with detection thresholds smaller than 40 Pa is clearly larger. For Mt. Etna, thresholds are invariant during summer, as no stations have better coverage than IS48. However, in winter, thresholds are reduced by a factor of 4 due to the favourable geographical locations of AMT in Italy, IPLOR in Romania and IMAR in Israel relative to the volcano.

In order to quantify this improvement over the year, Fig. 2(b) presents the cumulative histogram of the percentage of the covered

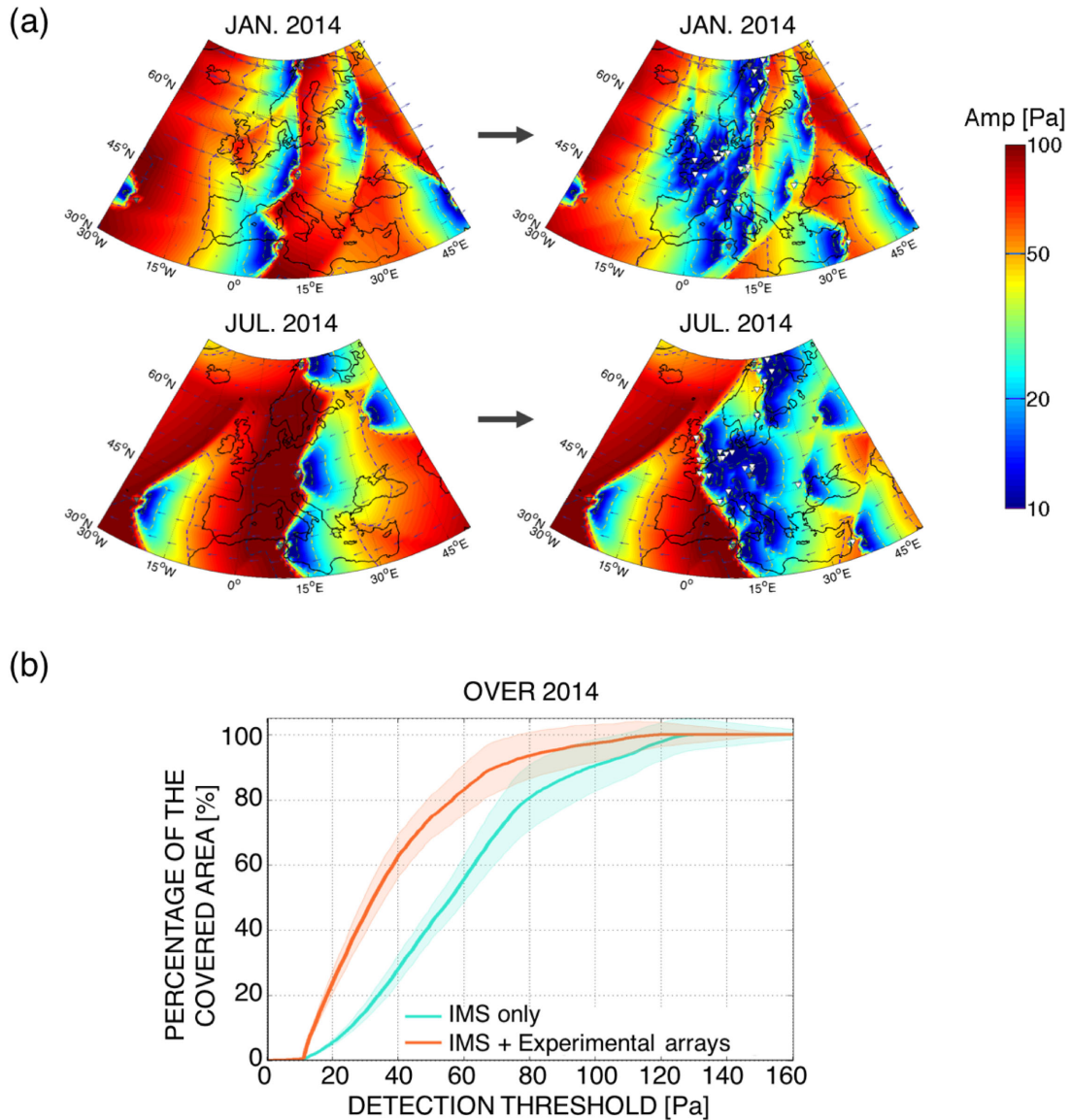


Figure 2. Quantification of infrasound network detection capabilities in the Euro-Mediterranean region when adding experimental arrays to the IMS network (2014). (a) Comparison of the smallest detectable source amplitude at 0.8 Hz considering one-station coverage. The colour codes the minimum detectable source amplitude at a reference distance of 1 km from the source (in Pa peak-to-peak). White and grey triangles indicate IMS and national arrays, respectively. Simulations were carried out with atmospheric conditions (blue arrows: wind direction) averaged over 2014 January (top) and over 2014 July (bottom) with the IMS network only (left) completed by experimental arrays (right). (b) Cumulative histogram of the percentage of the covered area versus detection thresholds. (IMS network: blue line and experimental arrays: orange line). Shaded error bars show the 95 per cent distribution interval throughout the year.

area for a given detection threshold. We consider the IMS network only and completed with the experimental stations. Adding stations to the network can improve performance by a factor up to 2. For example, to monitor 90 per cent of the covered region, incorporating the experimental arrays reduces the thresholds from ~ 100 to ~ 50 Pa. Such quantification studies are essential to understand the network performance and prioritizing geographical areas where network maintenance is necessary.

Simulating the infrasound network performance

We only consider detections associated to Mt. Etna, in the frequency range (0.8–2.5) Hz, with wave speed between 310 and 450 m s^{-1} , in a bandwidth of $\pm 10^\circ$ around the theoretical azimuth from IS48 to Etna. The resulting detection list is further reduced from outliers

by limiting the considered detections for a 6 h time window to a normal distribution around the average values, with a 90 per cent confidence interval. Time intervals with less than one detection per hour are not considered. A moving average of 24 h every 6 h is then realized. The resulted detections, expressed in terms of sound pressure level, at the IS48 station is compared to the ones at ETN (Fig. 3a; Assink *et al.* 2014a).

While near-field data are useful to constrain the source activity, far-field observations provide information on atmospheric conditions along propagation paths. At a distance of about 550 km, Etna is well monitored by IS48 from May to September during the downwind season. It is occasionally detected in winter during weeks following stratospheric wind reversals (Assink *et al.* 2014b; Smets & Evers 2014). During downwind conditions, an overall first-order agreement between the detecting periods at ETN

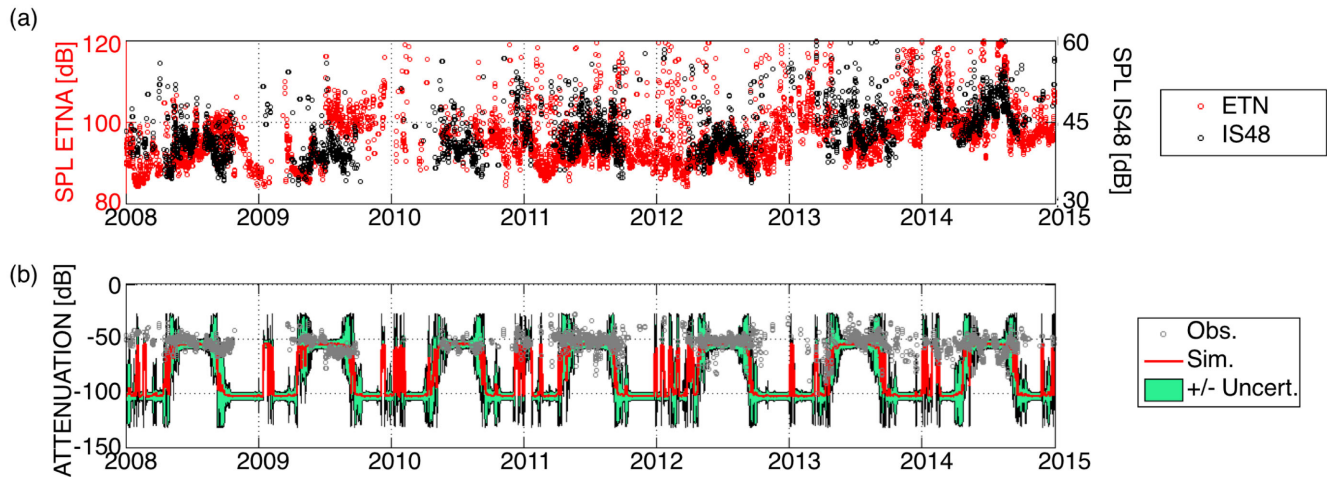


Figure 3. Simulated detection capability at IS48 using Mt. Etna infrasound signals observed at ETNA (2008–2015). (a) Comparison between the sound pressure level (SPL) measured at Mt. Etna (in red dots, corrected for spreading to 1 km) and IS48 (in black dots). During summer, the downwind periods favour long-range propagation of signals from Mt. Etna, with a constant attenuation of -50 dB. (b) Comparison between the simulated wave attenuation (red curve) and the one derived from near- and far-field observations (grey dots). Simulations are carried out at the dominant frequency of the recorded signals (1.6 Hz). Green areas delimit the 95 per cent confidence interval of the predicted attenuation when including 10 m s^{-1} wind speed random perturbations at stratospheric altitudes. During the equinoxes, larger detection periods are noted when incorporating these uncertainties.

and IS48 is noted, which emphasizes the capability of infrasound techniques to remotely monitor volcanic eruptions. The effects of minor sudden stratospheric warming (SSW) events, such as in 2011 January, are clearly visible when the locally reversal of the stratospheric wind direction favoured detections at IS48 (Assink *et al.* 2014b). This type of events arises due to near-splitting conditions. The detections at IS48 can also be noted when the direction of the stratospheric circumpolar vortex reverses from eastward (winter) to westward (summer) and vice versa during the equinox periods and major SSWs such as 2009 January and 2013 (Evers & Siegmund 2009; Coy & Pawson 2015). Therefore, detections at IS48 result from favourable summertime and occasionally during anomalous wintertime conditions.

In order to validate our method, we compare the predicted wave attenuation, simulated at a characteristic frequency of Mt. Etna (i.e. 1.6 Hz), with the one deduced from near- and far-field measurements (Fig. 3b). According to the previous campaign measurements under the ARISE project, we also consider 5 per cent of wind perturbations (i.e. $\sim 10 \text{ m s}^{-1}$) in the atmospheric specifications, which accounts for wind fluctuations that are not resolved by actual meteorological models. Considering the whole period, there is a good agreement between predictions and observations that suggest in most cases the propagation through stratospheric waveguides. During summer, comparable attenuation signals are constantly generated by Mt. Etna (i.e. -50 dB), which is coherent with the stable number of detections at IS48. Moreover, while the effects of adding a perturbation term in $C_{\text{eff-ratio}}$ are limited when winds prevail, they dominate when stratospheric winds reduce and reverse. Incorporating these uncertainties leads to a significant improvement in propagation modeling, which enlarges the detection periods by several weeks and resolves reasonably well the issue of unpredicted detections (Fig. 3b).

Optimizing the infrasound network performance

The optimization procedure was applied to the Euro-Mediterranean region in order to optimize the monitoring of Mt. Etna over one year. The objective was to find the optimized location of one additional array in order to improve the coverage of the existing network.

The improvement factor F_M (eq. 4), which is shown on Fig. 4(a), highlights the contribution of each position of the new station on Mt. Etna monitoring, over the year of 2014. To improve the network detection capabilities 50 per cent of the time, we need to set the new station on the east coast of the Adriatic Sea. However, Greece still represents a good location to add a new station to improve the network performance by at least a factor of 2 ($F_M > 2$) (Fig. S1, Supporting Information).

Under the ARISE project, other experimental stations provide additional remote recordings of Mt. Etna, such as AMT (42.87°N , 11.65°E) in Tuscany, at a distance of 640 km from the volcano. According to Figs 2(a) and 4(a), these stations can also supplement observations from Mt. Etna. In order to quantify the effect of adding these stations to the IMS network on the volcano monitoring, Fig. 4(b) presents the cumulative histogram of the percentage of time during one year, when Mt. Etna is detected with a given detection threshold. We consider the IMS network only and completed with the experimental stations. As expected, adding the stations allows to increase the detection periods by 40 per cent. We compare the contribution of these experimental stations to the IMS network performance during the periods of summer and winter (Figs S2a and b, Supporting Information). The detection capability of the whole network is only improved during winter due to preferential location of IS48 relative to Mt. Etna in summer. The observations are in good agreement with the remarks on Fig. 2(a).

Validation using repetitive volcanic infrasound from Mt. Yasur, Vanuatu

To further evaluate our method, we also consider Mt. Yasur (19.53°S ; 169.44°E) as another volcanic source of repetitive signals. This volcano is located on the island of Tanna, in the Vanuatu. Its persistent explosivity and its easy access make it one of the most studied volcanoes with 20-yr geophysical observations (Nabyl *et al.* 1997; Marchetti *et al.* 2013). Given the persistent explosivity and easy access, visual observations and direct measurements in the near field are often compromised due to cloud coverage and to unfavourable meteorological conditions. In this context, the

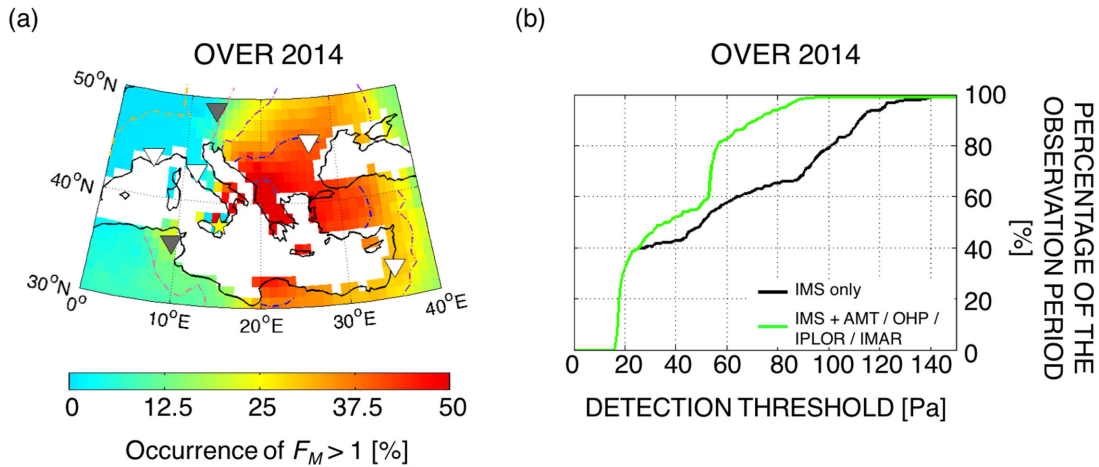


Figure 4. Optimization of the European infrasound network detection capabilities to detect Mt. Etna activity over 2014, at a frequency of 1.6 Hz. (a) Contribution of each geographical position for the new station to monitor Mt. Etna (yellow star), in addition to the IMS network over 2014. We consider one-station coverage. The colour codes the percentage of time over the year 2014, during which the considered position for the new station improve detection capabilities. We consider every location that would enhance the performance ($F_M > 1$). The grey and white reverse triangles indicate the location of IMS and experimental stations, respectively. (b) Cumulative histogram of the observation period of Mt. Etna, according to a specific detection threshold, during 2014. The black curve considers only the IMS network, that is to say IS48; the green curve presents the improvements of the network performance when adding experimental stations (AMT in Italy, OHP in France, IPLOR in Romania and IMAR in Israel).

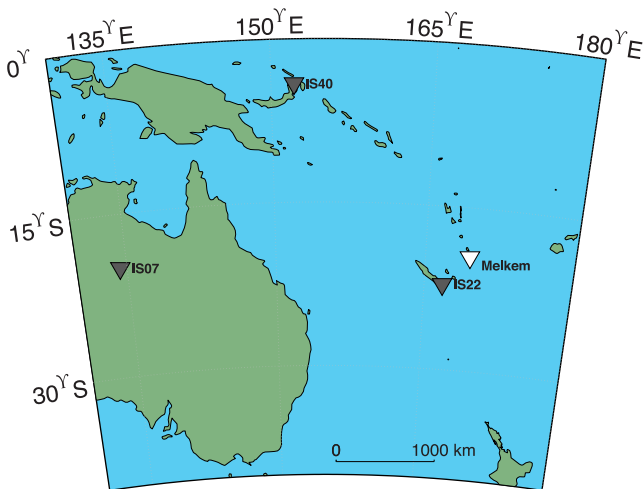


Figure 5. Geographical locations of stations used in this study. Grey and white reverse triangles indicate IMS and national arrays, respectively. Melkem station is located less than 5 km from the Mt. Yasur volcano.

infrasound technology represents a way to provide crucial information on the eruptive dynamics (Le Pichon *et al.* 2008; Marchetti *et al.* 2013).

Observation network

Since 2003, the infrasound IMS station in New-Caledonia (IS22, 22.18°S, 166.85°E) permanently detects coherent signals from different sources and especially from Mt. Yasur (Antier *et al.* 2007; Fig. 5). Such as for the IS48 station, processing of the IS22 data is performed using the PMCC algorithm. Near-field infrasound signals are recorded by the Melkem station, located at 500 m from the crater of the volcano since 2006. This station continuously detects infrasound generated by Mt. Yasur except during several periods when it was breakdown.

Simulating the infrasound network performance

Following the same procedure as for Etna, we evaluate the detection capability of IS22 until detect Mt. Yasur, from 2006 to now. We only consider detections associated to the volcano, in the frequency range (1–4) Hz (Antier *et al.* 2007), with wave speed between 310 and 450 m s⁻¹, in a bandwidth of $\pm 10^\circ$ around the theoretical azimuth from IS22 to Yasur. The outliers are suppressed through specific filtering. We limit the considered detections for a 6 h time window to a normal distribution around the average values, with a 90 per cent confidence interval. Time intervals with less than one detection per hour are not considered. A moving average of 24 h every 6 h is then realized (Assink *et al.* 2014a). The resulted detections, expressed in terms of sound pressure level, at the IS22 station is compared to the ones at Melkem (Fig. 6a). Detections of Mt. Yasur at IS22 are remarkable as they emphasize the systematic azimuthal trend, due to the seasonal oscillation of stratospheric winds. According to the geographical disposition of IS22 relative to the volcano, the stratospheric wind directivity explains the constant number of detections at the station during the austral summer. On the opposite, during the austral winter, the performance of IS22 is variable due to the perturbations in the atmosphere that give rise to occasional detections.

We compare the predicted wave attenuation, simulated at a characteristic frequency of Mt. Yasur (near 2 Hz), with the one deduced from near- and far-field measurements (Fig. 6b). We also consider 5 per cent of wind perturbations in the atmospheric specifications. Considering the whole period, same remarks can be made as the ones made for Mt. Etna. There is a good agreement between predictions and observations during downwind conditions even if the predicted attenuation is ~ 10 dB smaller than the observed one. When adding the perturbation term, we enlarge the simulated periods of detections especially during the equinoxes which better explain the previously unpredicted observations. Moreover, during downwind conditions, it leads to a better agreement between simulated and observed attenuation values.

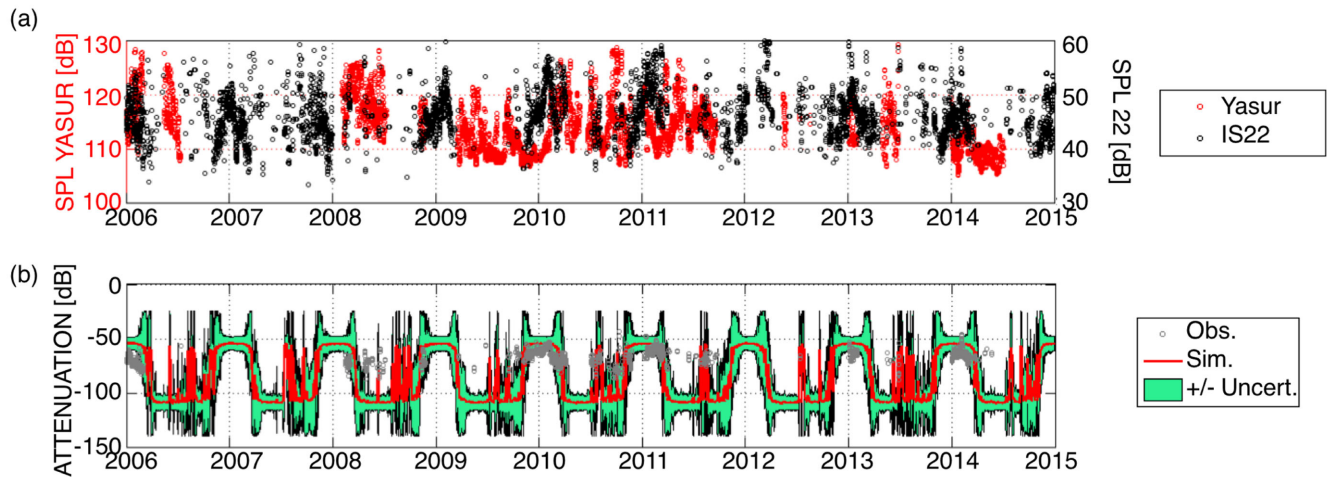


Figure 6. Simulated detection capability at IS22 using Mt. Yasur infrasound signals observed at Melkem (2006–2015). (a) Comparison between the sound pressure level (SPL) measured at Mt. Yasur (in red dots, corrected for spreading to 1 km) and IS22 (in black dots). During austral summer, the downwind periods favour long-range propagation of signals from Mt. Yasur, with a constant attenuation of -70 dB. (b) Comparison between the simulated wave attenuation (red curve) and the one derived from near- and far-field observations (grey dots). Simulations are carried out at the dominant frequency of the recorded signals (2 Hz). Green areas delimit the 95 per cent confidence interval of the predicted attenuation when including 10 m s^{-1} wind speed random perturbations at stratospheric altitudes. During the equinoxes, larger detection periods are noted when incorporating these uncertainties.

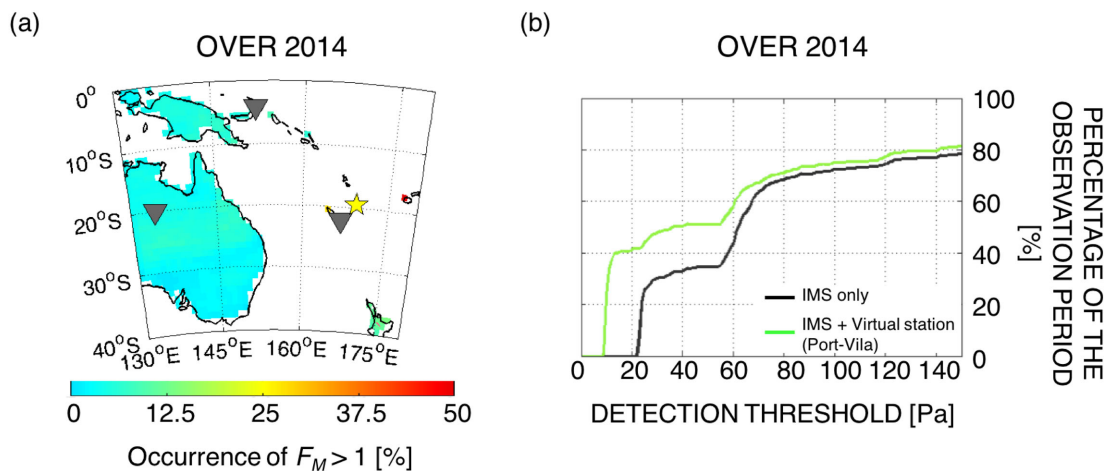


Figure 7. Optimization of the east-Australian infrasound network detection capabilities to detect Mt. Yasur activity over 2014, at a frequency of 2 Hz. (a) Contribution of each geographical position for the new station to monitor Mt. Yasur (yellow star), in addition to the IMS network over 2014. We consider one-station coverage. The colour codes the percentage of time over the year 2014, during which the considered position for the new station improve detection capabilities. We consider every location that would enhance the performance ($F_M > 1$). The grey reverse triangles indicate the location of IMS stations. (b) Cumulative histogram of the observation period of Mt. Yasur, according to a specific detection threshold, during 2014. The black curve considers only the IMS network, that is to say IS22; the green curve presents the improvements of the network performance if we add one experimental station at Port Vila.

Optimizing the infrasound network performance

We apply our method to the IMS network to optimize its performance to better monitor Mt. Yasur over the year. The improvement factor F_M (eq. 4), which is shown in Fig. 3(a), highlights the contribution of all candidate stations to monitor Mt. Yasur, over the year of 2014. Adding a new station in the Fiji would improve the detection capability by 50 per cent of the time (Fig. 7a). As opposed to Mt. Etna, the possibilities of locating new stations are limited due to the large oceanic coverage.

Fig. 7(b) presents the cumulative histogram of the percentage of time during the year of 2014, when Mt. Yasur is detected with a given detection threshold. A station at Port-Vila could reasonably well-supplement observations of the volcano, allowing a longer period of monitoring especially while ensuring low detection thresholds.

For example, if we consider a detection threshold of 40 Pa, adding a station at Port-Vila would improve the IMS network performance by a factor of 2. As for Mt. Etna detected by IS48, IS22 well detects Mt. Yasur during summer, due to its geographical position relative to the volcano. The contribution of the new station would only be effective in winter. Moreover, according to Fig. 7(b), the station at Port-Vila would not be able to cover time periods when detection thresholds are the highest, as both curves meet in this context.

DISCUSSIONS

In this study, we have presented two evaluations of our method. In a context of validation, two distinct volcanoes, Mt. Etna in Sicily and Mt. Yasur in Vanuatu, located respectively in the Northern and

Southern Hemispheres, have been considered. Their constant activity and their accessibility allowed us to combine near-field data with remote recordings. The locations of Mt. Etna and Mt. Yasur in the Northern and Southern hemispheres, respectively, allow to enlarge the validation of our simulation tool at a global scale, by considering more realistic propagation scenarios. An overall good agreement is found between simulations and observations. However, in both cases, some misfits between simulations and observations [i.e. a difference of ~ 10 dB in summer 2009 for Mt. Etna (Fig. 3b) and in austral summer 2010 for Mt. Yasur (Fig. 6b)] are noted. The latter could be due to local changes in the nature of the source explosive activity which leads to different infrasound characteristics such as the frequency content (Ripepe *et al.* 2009). In our simulations, we only consider one representative frequency (i.e. 1.6 Hz for Mt. Etna and 2 Hz for Mt. Yasur). However, the infrasound signals generated by these volcanoes rather present a large range of frequencies depending on the source processes. By considering losses for 1, 2 and 3 Hz, we can show that the 10 dB discrepancies between simulations and observations correspond to this frequency range (1–3 Hz (Fig. S3, Supporting Information)). Such difference could also be explained by the fact that we linearly corrected near-field infrasound signal with the distance. In this range, effects of topography and strongly variable atmospheric conditions can also significantly affect detections (de Angelis *et al.* 2012; Lacanna & Ripepe 2012; Dabrowa *et al.* 2014; Lacanna *et al.* 2014). Future studies could involve better analysis of the complex local and regional propagation, such as tropospheric or thermospheric returns. In fact, while our method does not account for tropospheric ducting, the high-frequency content of the considered volcanic signals does not favour thermospheric arrivals. Our method could be optimized to account for these effects to model more realistic propagation scenarios.

Moreover, more detections are sometimes found in the far-field compared to what is measured in the near field (i.e. during summer 2010 in Fig. 3a and during austral summer 2009 in Fig. 6a). This can be explained by the criteria used to select the detections related to each considered volcano (e.g. frequency range, trace velocity, etc.). For example, we consider a bandwidth of $\pm 10^\circ$ around the theoretical azimuth between the volcano and the station, which is large enough to include other signals than the considered volcanoes in our studies. In the case of Mt. Etna, such an azimuth range will cover both Mt. Etna and the nearby volcano of Mt. Stromboli.

When simulating the performance of infrasound networks, we have noted that the winter vortex is much stronger than the summer vortex. However, even if the propagation efficiency is better in winter, the detection capability is better in summer. This could be explained by higher noise levels in winter when compared to the summer. Moreover, if we focus on the detections of Mt. Etna by IS48, we can emphasize higher detection thresholds in winter. This could be influenced by either the reversal of the circumpolar vortex, leading to unfavourable stratospheric propagation or higher noise levels in winter at the station.

By considering a 5 per cent perturbation term in $C_{\text{eff-ratio}}$, we have been able to improve the agreement between observations and simulations, especially during the equinoxes. We found that these uncertainties cannot account for all unpredicted detections. During the ARISE campaign measurements, it has been shown that the differences between NWP models and observations are variable with time. For example, these perturbations could be strengthened to 40 m s^{-1} during some periods of the years, such as in summer 2009 for Mt. Etna (Fig. 3b), in order to better explain the still significant amount of uncovered predictions (Assink *et al.* 2014a). However,

the comparisons undertaken during the ARISE project only consider point measurements with spatially and temporally averaged ECMWF model values. Instead of fixing a constant value of perturbations in effective sound speeds, future studies could integrate realistic uncertainties that are dependent on the time and the space. Also, only the deterministic ECMWF model is used. There is an ensemble of models that could equally well be used (Smets *et al.* 2015).

Such study highlights the potential of the infrasound technology to remotely monitor volcanic eruptions. During downwind conditions between the volcanoes and the considered remote stations (i.e. Mt. Etna and IS48, Mt. Yasur and IS22), constant values of attenuation are both simulated and observed (i.e. -50 dB for Mt. Etna and -60 dB for Mt. Yasur), which is coherent with the stability in the number of detections at the respective stations. Moreover, when Melkem was out from 2006 to 2008, we can clearly emphasize the benefit of infrasound for remote monitoring purposes (Figs 6a and b). First, during the austral summer 2006–2007, Yasur is well detected by IS22 as the westward jets favour detections of low-attenuated signals from the volcano (i.e. -50 dB). Then, during the austral winter 2007, which is characterized by upwind conditions, recordings of Mt. Yasur are sparse due to the relatively high attenuation of the signals. Detections are noted only during minor or major SSW events, when winds reverse and favour infrasound propagation toward the IS22 station. Finally, at the beginning of 2008, signals from Mt. Yasur were neither detected by Melkem nor by IS22, which can be explained by a non-activity of the volcano during this period. In this context, the use of infrasound is essential for remotely monitoring volcanoes especially when near-field observations are not available. It is all the more essential as explosive eruptions can eject a large amount of ash in the atmosphere which is a direct threat to air traffic and to local communities.

In this study, we mainly assess the ability of one arbitrary infrasound network to detect volcanic activity in a specific region. We consider one-station coverage as we suppose the volcano position to be well known. However, for location purpose, we could extend our study for a two-station coverage, which is the baseline condition, or even for a three-station coverage, which gives the opportunity to reduce false alarm and to improve location accuracy.

Besides the ability of infrasound to provide a precise chronology of the volcanic eruption (Matoza *et al.* 2011a), some parameters such as the source amplitude could be extracted from the infrasound signal and could inform on the geophysical processes of the eruption. To do so, a robust evaluation of the capabilities of a network to monitor volcanic eruptions is required. By combining realistic atmospheric specifications with robust propagation models, our method leads to a reliable estimation of the infrasound detection capabilities. For example, Indonesia, in east Asia, is characterized by a strong volcanic activity. Thus, volcanic monitoring is of prime importance. In 2014 February, the eruption of the Kelud (7.93°S , 112.31°E) has attested the use of remote infrasound signals to rapidly detect volcanic explosions and to help defining eruption sequences (Caudron *et al.* 2015). It is thus fundamental to well constrain infrasound propagation from the source to the station in order to better characterize the source mechanism.

Such study clearly points out the efficiency of our method to assess and optimize the performance of any arbitrary infrasound network to monitor volcanic eruptions. We could also extend this work to monitor other types of source. It could be any virtual point source or even a region. In this context, our simulation tool presents

an interest for monitoring purposes in many kind of applications either scientific, or academic.

CONCLUSIONS

The network performance simulations presented in this study incorporate frequency-dependent semi-empirical attenuation relations, time-varying station noise, a realistic description of the spatio-temporal variability of the atmosphere and a first-order effective sound speed uncertainty in the stratopause region. These effects control to first order where infrasound signals are expected to be detected.

Quasi-permanent signals from Mt. Etna recorded by IS48 in Tunisia and from Mt. Yasur detected by IS22 in New Caledonia were used as a benchmark case study for evaluating the simulation results. A general good agreement is found between the modeled and observed results, except when the atmosphere is in a state of transition. These results emphasize the capability of infrasound techniques to remotely monitor volcanic eruptions. Including wind uncertainties where the mean state of ECMWF model and its variability are possibly inaccurate better explains unpredicted arrivals at IS48 and at IS22.

Quantitative investigation techniques explore theoretical scenarios aiming at optimizing the infrasound network performance over both the Euro-Mediterranean and the east Australian regions to respectively monitor Mt. Etna and Mt. Yasur. It has been shown that the detection thresholds can be lowered throughout the year by adding one array at appropriate location (Figs 4 and 7), especially where the station coverage is poor due to seasonally dependent propagation directivity. Such studies could help to define an optimal infrasound network to ensure permanent detection of a specific volcanic region and also for source location purpose.

Beyond the context of the future verification of the CTBT, continuing such studies is helpful to promote the potential benefits of infrasound monitoring techniques for civil and scientific applications. It provides in near real-time a realistic measure of the network performance and is useful to prioritize maintenance and optimize future network design. In particular, such investigations are of considerable value for providing reliable source information and chronology of the eruptive processes on active volcanoes from local to long-range observations (Dabrowa *et al.* 2011; Fee & Matoza 2013; Tailpied *et al.* 2013; Mialle *et al.* 2015). The use of infrasound to remotely observed volcanoes is also clearly highlighted in passive acoustic remote sensing of atmosphere analysis (Assink *et al.* 2014a; Le Pichon *et al.* 2015) and forecast models (Smets *et al.* 2016). The potential of infrasound is all the more promising if we combine other measurements such as seismic recordings with this technique. The implementation of such simulation tool into automated eruption detection systems could lead to substantial improvements in infrasound monitoring of remote volcanic regions and provide valuable observations to prevent eruption disasters and mitigate the impact of ash clouds on aviation.

ACKNOWLEDGEMENTS

All the data used in this work were collected by the University of Firenze, by IS48 in Tunisia and by the National Center of Cartography and Remote sensing of Tunis in Tunisia. This work was partly performed during the course of the ARISE design study project, funded by the Seventh Framework Programme (FP7) of the European Union (grant no. 284387) and the ARISE2 project within H2020, project no. 653980.

REFERENCES

- Antier, K., Le Pichon, A., Vergnolle, S., Zielinski, C. & Lardy, M., 2007. Multiyear validation of the NRL-G2S wind fields using infrasound from Yasur, *J. geophys. Res.*, **112**, D23110, doi:10.1029/2007JD008462.
- Assink, J.D., Le Pichon, A., Blanc, E., Kallel, M. & Khemiri, L., 2014a. Evaluation of wind and temperature profiles from ECMWF analysis on two hemispheres using volcanic infrasound, *J. geophys. Res.*, **119**, 8659–8683.
- Assink, J.D., Waxler, R., Smets, P.S.M. & Evers, L.G., 2014b. Bidirectional infrasonic ducts associated with sudden stratospheric warming events, *J. geophys. Res.*, **119**, 1140–1153.
- Bass, H., 1995. Atmospheric absorption of sound: further developments, *J. Acoust. Soc. Am.*, **97**(1), 680–683.
- Brachet, N., Brown, D., Le Bras, R., Mialle, P. & Coyne, J., 2010. Monitoring the Earth's atmosphere with the global IMS infrasound network, in *Infrasound Monitoring for Atmospheric Studies*, pp. 77–117, eds Le Pichon, A., Blanc, E. & Hauchecorne, A., Springer, Dordrecht, The Netherlands.
- Brown, D., Ceranna, L., Prior, M., Mialle, P. & Le Bras, R.J., 2014a. The IDC seismic, hydroacoustic and infrasound global low and high noise models, *Pure appl. Geophys.*, **171**, 361–375.
- Brown, D., Szuberla, C.A.L., McCormack, D. & Mialle, P., 2014b. The influence of spatial filters on infrasound array responses, *Pure appl. Geophys.*, **171**, 575–585.
- Campus, P. & Christie, D.R., 2010. Worldwide observations of infrasound waves, in *Infrasound Monitoring for Atmospheric Studies*, pp. 185–233, eds Le Pichon, A., Blanc, E. & Hauchecorne, A., Springer, Dordrecht, The Netherlands.
- Cansi, Y., 1995. An automatic seismic event processing for detection and location: the P. M. C. C. method, *Geophys. Res. Lett.*, **22**, 1021–1024.
- Caudron, C., Taisne, B., Garcés, M., Le Pichon, A. & Mialle, P., 2015. On the use of remote infrasound and seismic stations to constrain the eruptive sequence and intensity for the 2014 Kelud eruption, *Geophys. Res. Lett.*, **42**, 6614–6621.
- Christie, D.R. & Campus, P., 2010. The IMS infrasound network: design and establishment of infrasound stations, in *Infrasound Monitoring for Atmospheric Studies*, pp. 29–75, eds Le Pichon, A., Blanc, E. & Hauchecorne, A., Springer, Dordrecht, The Netherlands.
- Coy, L. & Pawson, S., 2015. The major stratospheric sudden warming of January 2013: analyses and forecasts in the GEOS-5 data assimilation system, *Mon. Weather Rev.*, **143**, 491–510.
- Dabrowa, A.L., Green, D.N., Johnson, J.B. & Rust, A., 2014. Comparing near-regional and local measurements of infrasound from Mount Erebus, Antarctica: implications for monitoring, *J. Volc. Geotherm. Res.*, **288**, 46–61.
- Dabrowa, A.L., Green, D.N., Rust, A.C. & Phillips, J.C., 2011. A global study of volcanic infrasound characteristics and the potential for long-range monitoring, *Earth planet. Sci. Lett.*, **310**, 369–379.
- De Groot-Hedlin, C.D. & Hedlin, M.A.H., 2014. Infrasound detection of the Chelyabinsk meteor at the USArray, *Earth planet. Sci. Lett.*, **402**, 337–345.
- De Angelis, S., Fee, D., Haney, M. & Schneider, D., 2012. Detecting hidden volcanic explosions from Mt. Cleveland Volcano, Alaska with infrasound and ground-coupled airwaves, *Geophys. Res. Lett.*, **39**, L21312, doi:10.1029/2012GL053635.
- De Groot-Hedlin, C.D., Hedlin, M.A.H. & Drob, D.P., 2010. Atmospheric variability and infrasound monitoring, in *Infrasound Monitoring for Atmospheric Studies*, pp. 475–507, eds Le Pichon, A., Blanc, E. & Hauchecorne, A., Springer, Dordrecht, The Netherlands.
- Donne, D. & Ripepe, M., 2012. High-frame rate thermal imagery of strombolian explosions: implications for explosive and infrasonic source dynamics, *J. geophys. Res.*, **117**, B09206, doi:10.1029/2011JB008987.
- Evers, L. & Haak, H., 2005. The detectability of infrasound in the Netherlands from the Italian volcano Mt. Etna, *J. Atmos. Sol. Terr. Phys.*, **67**, 259–268.
- Evers, L.G. & Siegmund, P., 2009. The infrasonic signature of the 2009 major sudden stratospheric warming, *Geophys. Res. Lett.*, **36**, doi:10.1029/2009GL041323.

- Evers, L.G. & Haak, H.W., 2010. The characteristics of infrasound, its propagation and some early history, in *Infrasound Monitoring for Atmospheric Studies*, pp. 3–27, eds Le Pichon, A., Blanc, E. & Hauchecorne, A., Springer, Dordrecht, The Netherlands.
- Fee, D. *et al.*, 2013. Overview of the 2009 and 2011 Sayarim infrasound calibration experiments, *J. geophys. Res.*, **118**, 6122–6143.
- Fee, D. & Matoza, R.S., 2013. An overview of volcano infrasound: from Hawaiian to plinian, local to global, *J. Volc. Geotherm. Res.*, **249**, 123–139.
- Garcés, M.A., Hansen, R.A. & Lindquist, K.G., 1998. Traveltimes for infrasonic waves propagating in a stratified atmosphere, *Geophys. J. Int.*, **135**, 255–263.
- Gibbons, S.J. *et al.*, 2015. The European arctic: a laboratory for seismoacoustic studies, *Seismol. Res. Lett.*, **86**, 917–928.
- Green, D.N. & Bowers, D., 2010. Estimating the detection capability of the International Monitoring System infrasound network, *J. geophys. Res.*, **115**, D18116, doi:10.1029/2010JD014017.
- Green, D.N., Le Pichon, A., Ceranna, L. & Evers, L., 2010. Ground truth events: assessing the capability of infrasound networks using high resolution data analyses, in *Infrasound Monitoring for Atmospheric Studies*, pp. 599–625, eds Le Pichon, A., Blanc, E. & Hauchecorne, A., Springer, Dordrecht, The Netherlands.
- Green, D.N., Vergoz, J., Gibson, R., Le Pichon, A. & Ceranna, L., 2011. Infrasound radiated by the Gerdec and Chelophechene explosions: propagation along unexpected paths, *Geophys. J. Int.*, **185**, 890–910.
- Hedlin, M.A.H. & Drob, D.P., 2014. Statistical characterization of atmospheric gravity waves by seismoacoustic observations, *J. geophys. Res.*, **119**, 5345–5363.
- Johnson, J.B. & Ripepe, M., 2011. Volcano infrasound: a review, *J. Volc. Geotherm. Res.*, **206**, 61–69.
- Kulichkov, S.N. & Golikova, E.V., 2011. Nonlinear effects manifested in infrasonic signals in the region of a geometric shadow, *Izv. Atmos. Ocean Phys.*, **49**, 77–81.
- Kulichkov, S.N., Chunchuzov, I.P. & Pupov, O.I., 2010. Simulating the influence of an atmospheric fine inhomogeneous structure on long-range propagation of pulsed acoustic signals, *Izv. Atmos. Ocean Phys.*, **46**(1), 60–68.
- Lacanna, G. & Ripepe, M., 2012. Influence of near-source volcano topography on the acoustic wavefield and implication for source modeling, *J. Volc. Geotherm. Res.*, **250**, 9–18.
- Lacanna, G., Ichihara, M., Iwakuni, M., Takeo, M., Iguchi, M. & Ripepe, M., 2014. Influence of atmospheric structure and topography on infrasonic wave propagation, *J. geophys. Res.*, **119**, 2988–3005.
- Lamb, O.D., De Angelis, S. & Lavallée, Y., 2015. Using infrasound to constrain ash plume rise, *J. Appl. Volcan.*, **4**(1), doi:10.1186/s13617-015-0038-6.
- Le Pichon, A. *et al.*, 2015. Comparison of co-located independent ground-based middle-atmospheric wind and temperature measurements with Numerical Weather Prediction models, *J. geophys. Res.*, **120**, doi:10.1002/2015JD023273.
- Le Pichon, A., Ceranna, L. & Vergoz, J., 2012. Incorporating numerical modeling into estimates of the detection capability of the IMS infrasound network, *J. geophys. Res.*, **117**, D05121, doi:10.1029/2011JD016670.
- Le Pichon, A., Vergoz, J., Herry, P. & Ceranna, L., 2008. Analyzing the detection capability of infrasound arrays in Central Europe, *J. geophys. Res.*, **113**, D12115, doi:10.1029/2007JD009509.
- Lingevitch, J.F., Collins, M.D. & Mills, M.J., 2002. A two-way parabolic equation that accounts for multiple scattering, *J. Acoust. Soc. Am.*, **112**(2), 476–480.
- Marchetti, E., Ripepe, M., Ulivieri, G., Caffo, S. & Privitera, E., 2009. Infrasonic evidences for branched conduit dynamics at Mt. Etna volcano, Italy, *Geophys. Res. Lett.*, **36**, L19308, doi:10.1029/2009GL040070.
- Marchetti, E., Ripepe, M., Delle Donne, D., Genco, R., Finizola, A. & Garaebiti, E., 2013. Blast waves from violent explosive activity at Yasur Volcano, Vanuatu, *Geophys. Res. Lett.*, **40**, 5838–5843.
- Matoza, R.S., Le Pichon, A., Vergoz, J., Herry, P., Lalande, J.M., Lee, H.I., Che, I.Y. & Rybin, A., 2011a. Infrasonic observations of the June 2009 Sarychev Peak eruption, Kuril Islands: implications for infrasonic monitoring of explosive volcanism, *J. Volc. Geotherm. Res.*, **200**, 35–48.
- Matoza, R.S. *et al.*, 2011b. Long-range acoustic observations of the Eyjafjallajökull eruption, Iceland, April–May 2010, *Geophys. Res. Lett.*, **38**, L06308, doi:10.1029/2011GL047019.
- Mialle, P. *et al.*, 2015. Towards a volcanic notification system with infrasound data, Oral T1.1-O4, in *Science and Technology 2015 Conference (CTBT Preparatory Commission)*, p. 15, 22–26 June, Vienna, Austria.
- Mutschlener, J.P. & Whitaker, R.W., 2010. Some atmospheric effects on infrasound signal amplitudes, in *Infrasound Monitoring for Atmospheric Studies*, pp. 455–473, eds Le Pichon, A., Blanc, E. & Hauchecorne, A., Springer.
- Nabyl, A., Dorel, J. & Lardy, M., 1997. A comparative study of low-frequency seismic signals recorded at Stromboli volcano, Italy, and at Yasur volcano, Vanuatu, New Zealand, *J. Geol. Geophys.*, **40**, 549–558.
- Norris, D., Gibson, R. & Bongiovanni, K., 2010. Numerical methods to model infrasonic propagation through realistic specifications of the atmosphere, in *Infrasound Monitoring for Atmospheric Studies*, pp. 541–573, eds Le Pichon, A., Blanc, E. & Hauchecorne, A., Springer, Dordrecht, The Netherlands.
- Pilger, C., Ceranna, L., Ross, J.O., Le Pichon, A., Mialle, P. & Garcés, M.A., 2015. CTBT infrasound network performance to detect the 2013 Russian fireball event, *Geophys. Res. Lett.*, **42**, 2523–2531.
- Ripepe, M., Delle Donne, D., Lacanna, G., Marchetti, E. & Ulivieri, G., 2009. The onset of the 2007 Stromboli effusive eruption recorded by an integrated geophysical network, *J. Volc. Geotherm. Res.*, **182**, 131–136.
- Ripepe, M., Bonadonna, C., Folch, A., Delle Donne, D., Lacanna, G., Marchetti, E. & Höskuldsson, A., 2013. Ash-plume dynamics and eruption source parameters by infrasound and thermal imagery: the 2010 Eyjafjallajökull eruption, *Earth planet. Sci. Lett.*, **366**, 112–121.
- Smets, P.S.M. & Evers, L.G., 2014. The life cycle of a sudden stratospheric warming from infrasonic ambient noise observations, *J. geophys. Res.*, **119**, 12 084–12 099.
- Smets, P.S.M., Evers, L.G., Näsholm, S.P. & Gibbons, S.J., 2015. Probabilistic infrasound propagation using realistic atmospheric perturbations, *Geophys. Res. Lett.*, **42**, doi:10.1002/2015GL064992.
- Smets, P.S.M., Assink, J.D., Le Pichon, A. & Evers, L.G., 2016. ECMWF SSW forecast evaluation using infrasound, *J. geophys. Res.*, **121**, 4637–4650.
- Sutherland, L.C. & Bass, H.E., 2004. Atmospheric absorption in the atmosphere up to 160 km, *J. acoust. Soc. Am.*, **115**, 1012–1032.
- Tailpied, D., Le Pichon, A., Marchetti, E., Ripepe, M., Kallel, M., Ceranna, L. & Brachet, N., 2013. Remote infrasound monitoring of Mt. Etna: observed and predicted network detection capability, *Inframatics*, **2**, 1–11.
- Ulivieri, G., Ripepe, M. & Marchetti, E., 2013. Infrasound reveals transition to oscillatory discharge regime during lava fountaining: implication for early warning, *Geophys. Res. Lett.*, **40**, 3008–3013.
- Vergnolle, S. & Brandeis, G., 1994. Origin of the sound generated by Strombolian explosions, *Geophys. Res. Lett.*, **21**, doi:10.1029/94GL01286.
- Whitaker, R.W., 1995. Infrasonic monitoring, in *Paper Presented at the 17th Annual Seismic Research Symposium, on Monitoring a Comprehensive Test-Ban Treaty (CTBT)*, LA-UR 95-2775, Los Alamos National Laboratory, 11–15 September, Scottsdale, Arizona.
- Woulff, G. & McGetchin, T.R., 1976. Acoustic noise from volcanoes: theory and experiment, *Geophys. J. Int.*, **1**, 601–616.

SUPPORTING INFORMATION

Additional Supporting Information may be found in the online version of this paper:

Figure S1. Contribution of each geographical position for the new station to monitor Mt. Etna (yellow star), in addition to the IMS network over 2014. We consider one-station coverage. The colour codes the percentage of time over the year 2014, during which the

considered position for the new station improve detection capabilities. We consider every location that would enhance the performance by at least a factor of 2 ($F_M > 2$). The grey and white reverse triangles indicate the location of IMS and experimental stations, respectively.

Figure S2. Cumulative histogram of the observation period of Mt. Etna, according to a specific detection threshold, during (a) winter and (b) summer 2014. The black curve considers only the IMS network, that is to say IS48; the green curve presents the improvements of the network performance when adding experimental stations (AMT in Italy, OHP in France, IPLOR in Romania and IMAR in Israel).

Figure S3. Comparison between wave attenuation simulated at different dominant frequencies: 1 Hz (in green), 2 Hz (in red) and 3 Hz (in blue). During the equinoxes, no difference is noted whereas during stable wind conditions (i.e. summer and winter), a discrepancy of 10 dB can be observed.

(<http://gji.oxfordjournals.org/lookup/suppl/doi:10.1093/gji/ggw400/-/DC1>).

Please note: Oxford University Press is not responsible for the content or functionality of any supporting materials supplied by the authors. Any queries (other than missing material) should be directed to the corresponding author for the paper.